Secondary-side-only Simultaneous Power and Efficiency Control by Online Mutual Inductance Estimation for Dynamic Wireless Power Transfer

Giorgio Lovison, Takehiro Imura and Yoichi Hori
The University of Tokyo
5-1-5 Kashiwanoha, Kashiwa, Chiba, 277-8561, Japan

Email: lovison@hflab.k.u-tokyo.ac.jp, imura@hori.k.u-tokyo.ac.jp, hori@k.u-tokyo.ac.jp

***Abstract* – Electric vehicles are an efficient alternative to gasoline-fuelled vehicles, but suffer from limited cruising range and long battery charging time. Wireless power transfer is among the solutions for these problems. By using it, the control of the power converters is essential for achieving high efficiency and desired power to the load at any time. Simultaneous regulation of both power and efficiency on the secondary side of WPT systems has already been proposed in past research. However, such control is still not verified in a dynamic scenario. Therefore, in this paper, the aforementioned control is applied to a dynamic charging scenario. The controllers are based on the online mutual inductance estimation, performed with recursive least square filter by constant trace algorithm. The experimental results show that the proposed control effectively works in dynamic charging.**

***Keywords* — Secondary side control, dynamic wireless power transfer, efficiency, power, mutual inductance.**

I. INTRODUCTION

Recently, electric vehicles (EVs) have been a popular research topic. In fact, they have notable advantages with respect to conventional vehicles such as low environmental impact, fast response and high torque delivery to the wheels. On the other hand, they currently suffer from limited cruising range, long battery charge time and higher cost.

With wireless power transfer (WPT) via magnetic resonant coupling [1] it is possible to overcome these problems. In fact, when applied to an electric vehicle, WPT allows battery charging of the electric vehicle while in motion as well as while stationary. However, an optimal power transmission requires a good converter control [2]. The most used types of control are power control and efficiency control and they are to be carried on either the wireless power system primary side [3][4], on the secondary side [5][6] or on both sides [7][8]. In a wireless power transfer system for battery charging, the secondary side include a AC/DC converter and a DC/DC converter connected to the load, a battery. Consequently, it is possible and desirable to regulate the efficiency and the power flow only by the converters in the secondary side while the primary side is not manipulated. The control performance in static charging scenario has already been proven [9][10]. Therefore, in this paper, the control is applied to a dynamic charging scenario. In order to maximize the transmission efficiency, an online estimation of the mutual inductance between the coils is needed. In this paper, the proposed mutual inductance estimation is performed by using only the secondary side information and adopted in the control.

More in detail, this paper is organized as follows. Section II explains the case of study. Section III presents the power and efficiency characteristics of WPT secondary side while section IV explains the concept of the control and illustrates the control operation and the choice of operation points. Section V discuss the simulation and experimental results. Section VI finally draws the conclusions from the results and suggests the future works.

II. CASE OF STUDY

This study focuses on the secondary side of a WPT system with series-series (SS) compensation, as shown in the equivalent circuit of Fig.1. The resonant frequency of the system is obtained from the coil parameters, which are independent from the load and the distance between the coils. The resonant angular frequency is expressed as:

$$\omega = \sqrt{\frac{1}{L_1 C_1}} = \sqrt{\frac{1}{L_2 C_2}} \tag{1}$$

with L_1 and C_1 as the primary coil inductance and capacitance, respectively; similarly, L_2 and C_2 are the secondary coil inductance and capacitance. The coils internal resistances only affect the losses and the dynamic response of the system. The mutual inductance L_m between the primary and secondary coil depends mainly on coil geometry. The values of these circuit parameters are listed in table I. In Fig.2 finally is shown the reference circuit: it includes a half active rectifier (HAR), a DC/DC converter

TABLE I. EXPERIMENTAL PARAMETERS OF THE COILS

Parameter	Value
Primary coil resistance R_1 [Ω]	1.82
Secondary coil resistance R_2 [Ω]	1.683
Primary coil capacitance C_1 [nF]	6.03
Secondary coil capacitance C_2 [nF]	12.15
Primary coil inductance L_1 [μH]	417.8
Secondary coil inductance L_2 [μH]	208.3
Mutual inductance L_m [μH] (best alignment)	37.9
Coil gap [mm] (best alignment)	100
Operating resonant frequency f_0 [kHz]	100

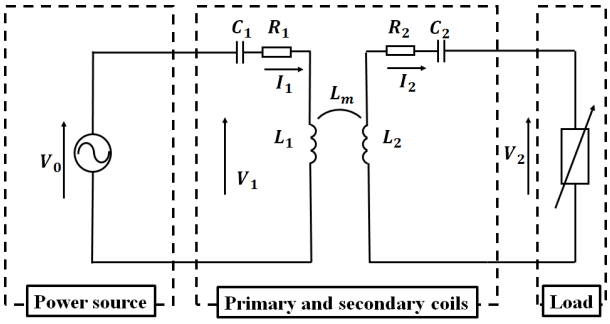

Fig. 1: Equivalent circuit of SS compensated WPT system.

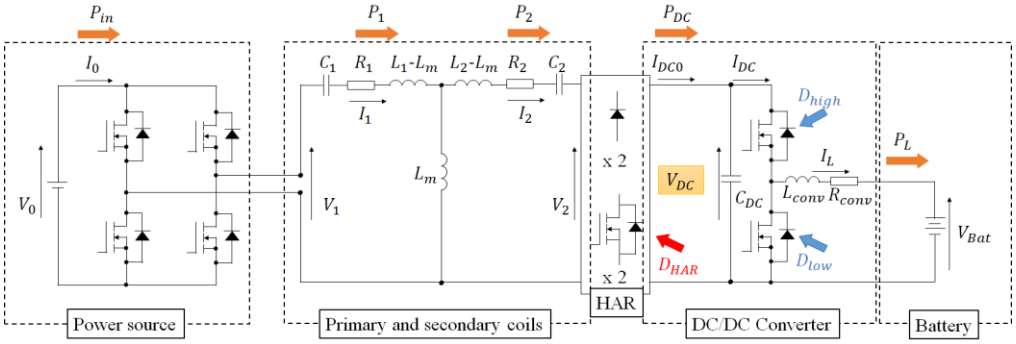

Fig. 2: Reference circuit of WPT using SS compensation and equivalent coil configuration.

and a battery as load. The proposed control strategy for the HAR and the DC/DC converter consists in the complementary modulation of the efficiency and the power flow only in the secondary side. The HAR and the DC/DC converter operate independently from the primary side converters without any kind of communication (e.g. Bluetooth). The motivation for controlling only the secondary side is to have an easier system to model and promote standardization of the primary side, considering a future scenario of widespread use.

III. CHARACTERISTICS OF WPT SYSTEM

In WPT theory, the formulae of the load power P_L and transmitting efficiency η, presented in previous papers such as [11]-[13], are given respectively by:

$$P_L = \frac{(\omega Lm)^2 Z_L}{\left[R_1(Z_L + R_2) + (\omega Lm)^2\right]^2} V_{1,0}{}^2 \tag{2}$$

$$\eta = \frac{(\omega Lm)^2 Z_L}{(R_2 + Z_L)\left[R_1(Z_L + R_2) + (\omega Lm)^2\right]} \tag{3}$$

where Z_L is the load impedance seen from the secondary coil, R_2 is the secondary coil resistance, R_1 is the primary coil resistance and $V_{1,0}$ is the rms value of the fundamental wave of primary side voltage, supposing the primary inverter is operated with a square wave voltage. In this

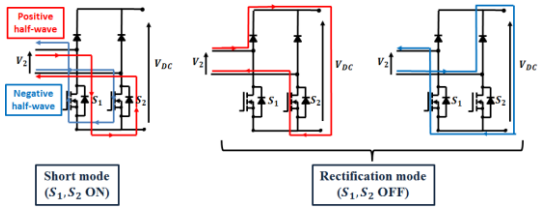

Fig. 3: HAR modes.

paper, the power factor of the primary side voltage is assumed to be unity, therefore the fundamental waves of the secondary side voltage V_2 and current I_2 are considered to be in phase. The HAR is a full wave diode bridge whose low side diodes are replaced by active devices like MOSFETs or IGBTs: by turning on the both the devices on the low side, the coil terminals are shorted (short mode) and no power is transmitted to the load. This is possible only because the SS compensation of magnetic resonant coupling makes the secondary side coil behave like an equivalent current source, thus allowing secondary side coil short circuit. On the other hand, if both the low side devices are off, the converter works like a conventional single-phase rectifier composed by diodes (rectification mode), as shown in Fig. 3, and power is sent to the load.

The influence of load impedance has been examined in past research [11][12][14]. In particular, the load impedance associated with maximum transmission efficiency and the one related to maximum deliverable power are different. The former one is equal to:

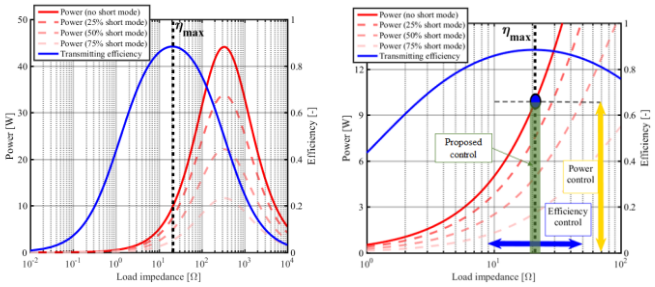

(a) Power and efficiency curves (b) Enlargement with operation range

Fig. 4: Transmission efficiency and load power with respect to load impedance for $V_1 = 18$ V and $L_m = 37.9\,\mu$H.

$$Z_{L,\eta\max} = \sqrt{\frac{R_2}{R_1}(\omega L_m)^2 + {R_2}^2} \tag{4}$$

The voltage that maximizes the transmission efficiency can be expressed by:

$$V_{\eta\max} = \sqrt{\frac{R_2}{R_1}}\frac{\omega L_m}{\sqrt{R_1 R_2} + \sqrt{R_1 R_2 + (\omega L_m)^2}} V_{1,0} \tag{5}$$

On the other hand, the load impedance and the voltage related to the maximum available power are respectively:

$$Z_{L,P\max} = \frac{(\omega L_m)^2}{R_1} + R_2 \tag{6}$$

$$V_{P\max} = \frac{\omega L_m}{2R_1} V_{1,0} \tag{7}$$

Voltages in (5) and (7) are rms values since the active power delivered to the load is related to the fundamental wave of the HAR input voltage V_2, which is a square wave. Finally, in order to send the required power with high transmission efficiency, the total input impedance seen from the secondary coil must be $Z_{L,\eta\max}$ during rectification mode.

IV. CONTROL CONCEPT AND OPERATION

The relationship between power and efficiency with respect to the load impedance is Fig. 4(a). The power corresponding to maximum transmitting efficiency is fixed, as highlighted in Fig. 4(b). However, with the proposed secondary side control, it is possible to send a different power value while retaining the same transmitting efficiency [9]. This is because of the HAR switching between short mode and rectification mode. The length of the short mode over the HAR switching period determines the amount of power received by the load.

In rectification mode, the rms value of secondary side voltage is unchanged because the DC/DC converter control keeps the voltage matched to the reference value. The secondary side coil behaves like an equivalent current source, thus the current does not change as well. Therefore, the rms value of the secondary side input power P_2 is unchanged. Consequently, by use of short mode, the desired power can be sent to the load with high efficiency without manipulating the primary side. The power, as well as the efficiency, is calculated by averaging; consequently, the averaged efficiency will be lower. In fact, during rectification mode the efficiency is maximum while in short mode it is zero since the load is not supplied. The modulation is done through short mode: the longer it is, the lesser the power received by the load. In short mode, there are certainly losses in the secondary side coil due to the circulating current; however, they are low because primary side power P_{in} becomes low.

In this paper, the following conditions are assumed:

1) Primary side coil voltage V_1 and system resonant angular frequency ω are known and fixed.
2) The HAR switching frequency is at least one order of magnitude slower than the DC/DC converter switching frequency to prevent conflicts.

In Fig. 5 and Fig. 6 are represented the control blocks for the HAR and DC/DC converter, respectively.

A. Control of HAR

The HAR operates a current control because the DC/DC converter regulates the secondary DC link voltage. Therefore, during rectification mode, its equation can be expressed as [15]:

$$I_{DC0} = \frac{2\sqrt{2}}{\pi} I_2 \tag{8}$$

However, since short mode must be included, the average value of I_{DC0} along the HAR switching period must be considered. Therefore, the average value can be derived from (8) as follows:

$$\bar{I}_{DC0} = \frac{2\sqrt{2}}{\pi} I_2 (1 - D_{HAR}) \tag{9}$$

The average power P_{DC} is obtained by rearranging (9) into:

$$P_{DC} = V_{DC}\bar{I}_{DC0} = P_2(1 - D_{HAR}) \tag{10}$$

The equation in (10) can be considered the linearized plant of the HAR P_{HAR}. Given the order of the latter, a PI controller $C_{PI}(s)$, expressed in (11), is deemed sufficient.

$$C_{PI}(s) = k_{p,PI} + \frac{k_{i,PI}}{s} \tag{11}$$

In order to set the feedforward part for the power control, a voltage formula related to the desired power P_L^* and the maximum power is necessary. From (7), such voltage is computed as follows [16]:

$$V_{P_L^*} = V_{P\max} - \sqrt{{V_{P\max}}^2 - \frac{\left[R_1 R_2 + (\omega L_m)^2\right] P_L^*}{R_1}} \tag{12}$$

By rearranging (12), the value of the desired power P_L^* as a function of the voltage is obtained as follows:

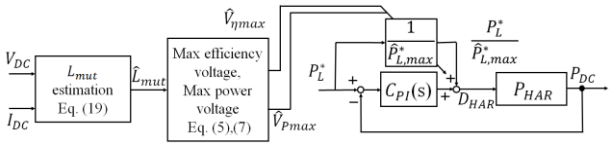

Fig. 5: HAR power control block.

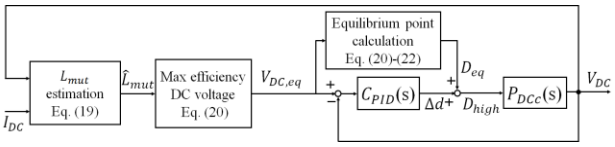

Fig. 6: DC/DC converter efficiency control block.

$$P_L^* = \frac{R_1\left[V_{P\max}{}^2 - \left(V_{P_L^*} - V_{P\max}\right)^2\right]}{R_1R_2 + (\omega L_m)^2} \tag{13}$$

The upper limit of the desired power is reached when $V_{P_L^*} = V_{\eta\max}$; therefore, (13) becomes:

$$P_{L,\max}{}^* = \frac{R_1\left[V_{P\max}{}^2 - \left(V_{\eta\max} - V_{P\max}\right)^2\right]}{R_1R_2 + (\omega L_m)^2} \tag{14}$$

With (14) the feedforward part of the control in Fig. 5 is set. It should be noted that $P_L^* \le P_{L,\max}{}^*$; if $P_L^* \ge P_{L,\max}{}^*$, it is necessary to increase V_1 and calculate again the parameters.

B. Online mutual inductance estimation

Since this paper deals with a dynamic charging scenario, the coils are moving and therefore the mutual inductance between them changes. Therefore, a method to estimate online the mutual inductance is necessary because many controller parameters depend on it. A real-time estimation of the coils coupling coefficient by means of a buck converter has already been proposed [17]. According to it, the mutual inductance can be expressed as follows:

$$\hat{L}_{mut} = \frac{V_{1,0} + \sqrt{V_{1,0}{}^2 - 4R_1I_2(V_2 + R_2I_2)}}{2I_2\omega} \tag{15}$$

The secondary side coil voltage V_2 and current I_2 are fundamental waves whose rms values are extracted respectively from V_{DC} and I_{DC} by Fourier series expansion. With a recursive least square (RLS) filter, the estimation error due to noise is reduced. However, the operation of HAR is an additional source of noise because of short mode. In fact, during short mode, the secondary DC link current is zero and the filter is not persistently excited. This leads to estimation windup, where the covariance matrix used for filter coefficients updating will inflate and greatly increase the sensitivity. In this condition, the estimation will be very inaccurate. Therefore, the RLS filter with constant trace algorithm is proposed to mitigate estimation mistakes due to enhanced sensitivity.

The proposed filter has its output $y[i]$ and input $\varphi[i]$ expressed as follows:

$$y[i] = V_{1,0} + \sqrt{V_{1,0}{}^2 - 4R_1I_2(V_2[i] + R_2I_2[i])} \tag{16}$$

$$\varphi[i] = 2I_2[i]\omega \tag{17}$$

with i as the sampling counter. From (16) and (17), the updating parameters and the mutual inductance estimation are computed in discrete time as:

$$\varsigma[i] = y[i] - (\varphi[i]\hat{L}_{mut}[i-1]) \tag{18}$$

$$\hat{L}_{mut}[i] = \hat{L}_{mut}[i-1] - \frac{\gamma\varphi[i]}{1+\varphi[i]^2}\varsigma[i] \tag{19}$$

with γ as a parameter incorporating the forgetting factor and the trace of the covariance matrix. The choice of γ is important for the correct estimation. If γ is too big, estimation windup happens; on the other hand, if γ is too small, a strong delay will occur and rapidly changing parameters will not be sensed properly.

C. Control of DC/DC converter

In the case of study, the DC/DC converter is a buck converter. In past research [17], the feedforward part of the controller represents the equilibrium point. The equilibrium values of V_{DC} and the load current I_L are given as follows:

$$V_{DC,eq} = \frac{V_{Bat}D_{eq} + R_{conv}I_{DC,eq}}{D_{eq}{}^2},\ I_{L,eq} = \frac{I_{DC,eq}}{D_{eq}} \tag{20}$$

where V_{Bat} is the battery voltage, D_{eq} is the feedforward part of the DC/DC converter high-side switch duty cycle and R_{conv} is the DC/DC converter resistance. The same can be derived for the equilibrium point of I_{DC} and D_{eq}:

$$I_{DC,eq} = \frac{8}{\pi^2}\frac{\omega L_m V_{1,0} - R_1V_{DC,eq}}{R_1R_2 + (\omega L_m)^2}(1 - D_{HAR}) \tag{21}$$

$$D_{eq} = \frac{V_{Bat} + \sqrt{V_{Bat}{}^2 - 4R_{conv}V_{DC,eq}I_{DC,eq}}}{2V_{DC,eq}} \tag{22}$$

The controller sets $V_{DC,eq}$ equal to maximum efficiency voltage $V_{\eta\max}$, as expressed in (5), multiplied by $\pi/2\sqrt{2}$. From that, all other equilibrium values are calculated. The buck converter transfer function is computed from the state space equations of the small signal model and is given by:

$$P_{DCc}(s) = \frac{\Delta V_{DC}}{\Delta d} = \frac{b_1s + b_0}{s^2 + a_1s + a_0} \tag{23}$$

$$a_1 = \frac{R_{conv}}{L_{conv}} + \frac{8}{\pi^2}\frac{R_1(1 - D_{HAR})}{C_{DC}\left[R_1R_2 + (\omega L_m)^2\right]}$$

$$a_0 = \frac{1}{L_{conv}C_{DC}}\left(D_{eq} + \frac{8}{\pi^2}\frac{R_{conv}R_1(1 - D_{HAR})}{R_1R_2 + (\omega L_m)^2}\right)$$

$$b_1 = -\frac{I_L}{C_{DC}}, \quad b_0 = -\frac{R_{conv} I_L + D_{eq} V_{DC}}{L_{conv} C_{DC}}$$

As (23) is a second-order transfer function, the feedback part is designed with PID controller through pole placement, expressed by:

$$C_{PID}(s) = k_{p,PID} + \frac{k_{i,PID}}{s} + \frac{k_{d,PID}\, s}{\tau s + 1} \tag{24}$$

V. Simulation and Experimental Results

In order to verify the effectiveness of the proposed method, simulations and experiments have been performed.. The experimental setup is shown in Fig. 7. It includes a DC generator (TAKASAGO ZX-400LA), the primary side inverter, primary and secondary coils, a HAR, a DC/DC converter, a DSP (Myway PE-PRO/F28335A) and a battery.

In the experiment, the receiver coil is moved by a linear actuator. The speed of the moving receiver coil is 10 km/h. The desired power is set to 4 W and the value of γ is 0.1. Other experiment parameters are shown in table II. The HAR closed loop poles are placed at -5 rad/s while the DC/DC converter ones are placed at -500 rad/s. The simulations are discussed with the experimental results of both the efficiency control as in [17] and the proposed one.

In Fig. 8, the simulation results are shown. In 8(a), the mutual inductance estimation is presented. With the proposed method, the mutual inductance estimation has little noise but is still not very accurate. Actually, the constant trace algorithm is conceived for steady state condition. However, before the transient of rectification mode can end, short mode happens, so that steady state is never achieved. However, in 8(b), the DC link voltage reference and V_{DC} are shown. The voltage reference is computed from the mutual inductance estimation, When the mutual inductance is too low, the actual value of V_{DC} diverges from the reference; otherwise, it is a match. As it can be seen from 8(c), the power reference value is 4 W and is matched by P_{DC}. When the mutual inductance is lower due to the coil movement, there is a power surge typical of dynamic charging. Otherwise, the reference is matched. In figure 8(d), the DC-to-DC efficiency is shown. The instant value presents many oscillations due to its computation being the ratio between secondary side power P_{DC} and primary side power P_{in}; however, the average value is near the maximum efficiency as expected.

In Fig. 9, the experimental results for the secondary side efficiency control [17] are presented. In 9(a), the estimation is quite accurate because the input of the estimation is always excited. Therefore, in 9(b), V_{DC} matches the reference produced from the estimation. As this is an efficiency control, the secondary power (blue line) in 9(c) is not regulated, therefore its change depends on the mutual inductance. Finally, in 9(d) the DC-to-DC efficiency is shown. Its value is the maximum efficiency achievable by the system under investigation.

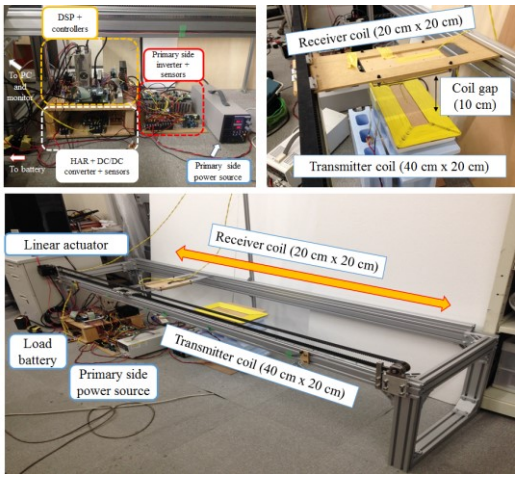

Fig. 7: Experimental setup.

TABLE II. Experimental Parameters of the System

Parameter	Value
Primary voltage source V_0 [V]	18
HAR switching frequency [kHz]	0.5
DC/DC converter switching frequency [kHz]	10
DC/DC converter resistance R_{conv} [Ω]	0.2
DC/DC converter capacitor C_{DC} [μF]	1000
DC/DC converter inductance L_{conv} [μH]	1000
Load battery voltage V_{Bat} [V]	6
System sampling period [μs]	20

The experimental results of the proposed control are reported in Fig. 10. In 10(a), the mutual inductance estimation is in agreement with 8(a), because there is an estimation error which tends to increase with time. However, despite the estimation error, in 10(b) the voltage reference is closely followed by V_{DC}. In 10(c) and 10(d), both the power profile and the DC-to-DC efficiency are in good agreement with the simulation results. As expected, the averaged DC-to-DC efficiency in 10(d) is slightly lower than the one in 9(d) because of short mode losses.

VI. Conclusion and Future Works

This paper proposed a simultaneous power and efficiency control performed only on the secondary side of a dynamic wireless power transfer system, without manipulating the primary side. Since the mutual inductance is unknown, an improved estimation based on constant trace algorithm is proposed. Experimental results confirm the validity of the proposed method.

Future works include high power experiment and improvement of mutual inductance estimation by system identification methods.

References

[1] A. Kurs, A. Karalis, R. Moffatt, J.D. Jonnopoulos, P. Fisher, M. Soljacic, “Wireless power transfer via strongly coupled magnetic

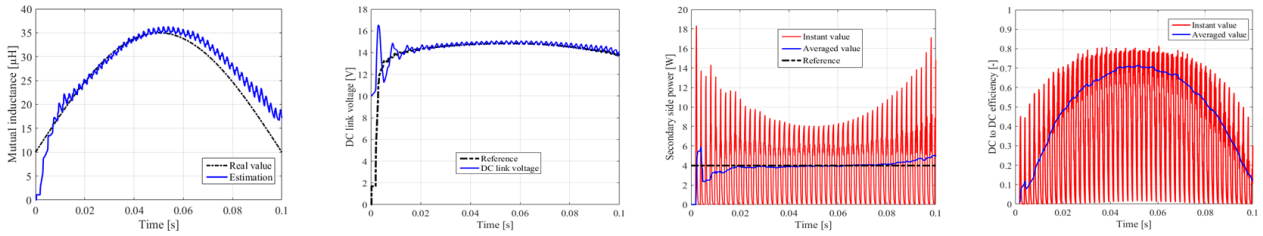

(a) Mutual inductance (b) DC link voltage (c) Secondary side power (d) DC to DC efficiency

Fig. 8: Simulation result with the proposed control for a speed of 10 km/h.

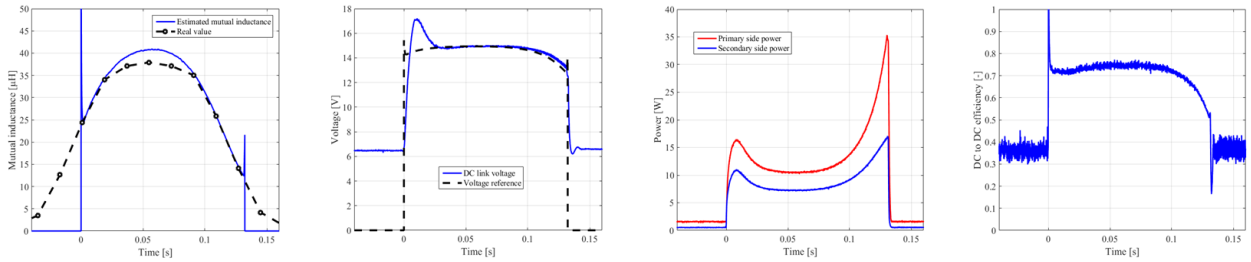

(a) Mutual inductance (b) DC link voltage (c) Power (d) DC to DC efficiency

Fig. 9: Experiment result with the efficiency control [17] for a speed of 10 km/h.

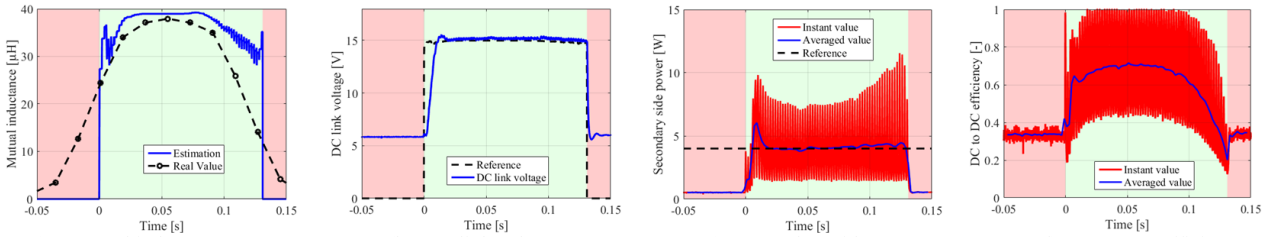

(a) Mutual inductance (b) DC link voltage (c) Secondary side power (d) DC to DC efficiency

Fig. 10: Experiment result with the proposed control for a speed of 10 km/h.

resonances", Science Expressions on 7 June 2007, Vol. 317, No. 5834, pp. 83-86, 2007.

[2] S. Li, C.C. Mi, "Wireless power transfer for electric vehicle applications", IEEE Journal of Emerging and Selected Topics in Power Electronics, pp. 1-14, 2013.

[3] H.L. Li, A.P. Hu, G.A. Covic, T. Chunsen, "A new primary power regulation method for contactless power transfer", IEEE International Conference on Industrial Technology (ICIT), pp. 1-5, 2009.

[4] J.M. Miller, C.P. White, O.C. Onar, P.M. Ryan, "Grid side regulation of wireless power charging of plug-in electric vehicles", IEEE Energy Conversion Congress and Exposition (ECCE), pp. 261-268, 2012.

[5] W. Chwei-Sen, O.H. Stielau, G.A. Covic, "Design considerations for a contactless electric vehicle battery charger", IEEE Transactions on Industrial Electronics, vol. 52, pp. 1308-1314, 2005.

[6] M. Fu, C. Ma, X. Zhu, "A cascaded boost-buck converter for high efficiency wireless power transfer systems", IEEE Transactions on Industrial Informatics, Vol. 10, No. 3, pp. 1972-1980, 2014.

[7] H.H. Wu, A. Gilchrist, K.D. Sealy, D. Bronson, " A high efficiency 5 kW inductive charger for EVs using dual side control", IEEE Transactions on Industrial Informatics, vol. 8, pp. 585-595, 2012.

[8] T. Diekhans, R. W. De Doncker, " A dual-side controlled inductive power transfer system optimized for large coupling factor variations" IEEE Energy Conversion Conference and Exposition (ECCE) 2014, pp. 652-659, 2014.

[9] G. Lovison, M. Sato, T. Imura, Y. Hori, "Secondary-side-only Control for Maximum Efficiency and Desired Power in Wireless Power Transfer System", Proc. 41st Annual Conference of the IEEE Industrial Electronics Society (IECON) 2015, pp. 4824-4829, 2015.

[10] K. Hata, T. Imura, Y. Hori, "Dynamic wireless power transfer system for electric vehicle to simplify ground facilities - power control and efficiency maximization on the secondary side ," The Applied Power Electronics Conference and Exposition, pp. 1731–1736, 2016.

[11] K. Hata, T. Imura, Y. Hori, "Maximum Efficiency Control of Wireless Power Transfer Considering Dynamics of DC-DC Converter for Moving Electric Vehicles", The Applied Power Electronics Conference and Exposition, pp. 3301-3306, 2015

[12] T. Hiramatsu, X. Huang, M. Kato, T. Imura, Y. Hori, "Wireless Charging Power Control for HESS Through Receiver Side Voltage Control", The Applied Power Electronics Conference and Exposition, pp. 1614-1619, 2015.

[13] M. Kato, T. Imura, Y. Hori, "New characteristics analysis considering transmission distance and load variation in wireless power transfer via magnetic resosnat coupling", IEEE Proceedings INTELEC, 2012.

[14] M. Kato, T. Imura, Y. Hori, "Study on maximizing efficiency by secondary side using DC-DC converter in wireless power transfer via magnetic resosnat coupling", The 27th International Electric Vehicle Symposium and Exhibition, pp. 1-5, 2013.

[15] D. Gunji, T. Imura, H. Fujimoto, "Operating Point Setting Method for Wireless Power Transfer with Constant Voltage Load", 41st Annual Conference of IEEE Industrial Electronics Society, pp.881-886, 2015.

[16] K. Hata, T. Imura, Y. Hori, "Dynamic Wireless Power Transfer System for Electric Vehicle to Simplify Ground Facilities - Power Control Based on Vehicle-side Information", The 28th International Electric Vehicle Symposium and Exhibition, pp. 1 – 12, 2015.

[17] D. Kobayashi, T. Imura, Y. Hori, "Real-time coupling coefficient estimation and maximum efficiency control on dynamic wireless power transfer for electric vehicles", 2015 IEEE PELS Workshop on Emerging Technologies: Wireless Power, pp. 1-6, 2015.